Assessing local statistics of a premixed turbulent Bunsen flame*

Yue Weng[†], Aditya Potnis[‡], Vishnu R. Unni[§], and Abhishek Saha[¶]
Department of Mechanical and Aerospace Engineering, University of California San Diego, La Jolla, CA - 92093, USA

The local interactions between the flamefront and turbulence control the dynamics, morphology, and propagation of a premixed turbulent flame. To investigate such complex dynamics of flame-turbulence interaction, we present an experimental exposition of a premixed turbulent Bunsen flame. Several quantities have been evaluated to assess the flame-turbulence interaction. We first measured the statistics of the flow field adjacent to the flame and compared it with the cold flow. This allowed us to evaluate the effect of the flame on the upstream turbulence. Subsequently, we performed statistical analyses of the local values of various stretch rates and quantified how their distribution changes with turbulence intensity and flame temperature. We also evaluated the pairwise relation between various stretch rates to assess their dependence on each other. Finally, we used flame particles to evaluate the Lagrangian evolution of stretch rates conditioned on flamefronts. All the analyses presented in this work point out Karlovitz number as a key factor in determining the flame-turbulence interaction. Specifically, we observe a stronger influence of turbulent eddies on flames with increasing Karlovitz number, as evidenced by the reduced effect of flame on upstream flow, wider PDFs of stretch rates, and increased persistence time scales for stretches.

I. Introduction

Turbulent combustion is ubiquitous in many practical devices, including gas turbines, rocket engines, automotive engines, and industrial burners. Due to the complexity arising from turbulence and its interaction with the combustion processes, turbulent combustion remains a challenging topic [1, 2]. A turbulent flow contains eddies of a multitude of lengths and timescales, which causes local unsteadiness. These eddies cause the wrinkling of a premixed flamefront within a turbulent flow, altering its shape and structure, which, in turn, results in the modification of several key behaviors, including transport process, propagation speed, fuel consumption rate, etc. [3]. Due to its importance in assessing the performance, stability, and reliability of combustors, a considerable amount of research has been conducted to quantify the global dynamics of turbulent flames, using theory, experiments, and numerical simulations [3–9].

^{*}A part of work was presented at the AIAA Aviation Forum 2023, June 12-16, San Diego, CA (Paper # AIAA 2023-3463)

[†]PhD Student

[‡]PhD Student

[§] Postdoctoral Researcher (UCSD), currently Asst. Professor at Indian Institute of Technology Hyderabad, India

[¶]Asst. Professor, AIAA Senior Member, Corresponding author. Email: asaha@ucsd.edu

The propagation of a premixed turbulent flame largely depends on the wrinkling caused by the turbulent eddies, altering the flamefront surface area and, thus, the burning rate [10, 11]. The degree of wrinkling on the flamefront is influenced by several factors, including characteristic length and time scales of flame and turbulence. By employing order-of-magnitude analyses of these scales, it can be shown that premixed turbulent flames can theoretically be categorized into several regimes with various structures and morphologies, as portrayed in the famous Borghi diagram [11, 12]. While this regime diagram is widely utilized for identifying the global dynamics of turbulent flames, researchers have experimentally and numerically demonstrated that local flame dynamics are more complex, with several exceptions reported in regime boundaries [13, 14]. Additionally, the flamefront cellular instabilities provide another mechanism for the wrinkling of local flamelets [15–17]. When accounted for, the effect of cellular instabilities leads to modified global dynamics, and hence, regime maps for premixed turbulent flames [18–20]. Consequently, understanding the local statistics of flamefronts becomes crucial to comprehend the competitive role of turbulence and instabilities in flame dynamics. Furthermore, the accuracy of Large Eddy Simulations (LES), wherein the flame and flow dynamics are resolved only to limited scales, depends on accurate sub-grid scale models that describe the physics in the scales not resolved in simulations [9]. These sub-grid scale models are constructed based on the physics of local flamefront dynamics.

Owing to its importance, the flamefront wrinkling and its effect on local flamelets were the focus of several numerical studies, where sub-grid scales models were proposed using the equilibrium assumption [21], conditional filtering [22], and fractal dimension of local flamelets [23]. Some studies also focused on the interaction of laminar flamelets and vortices to provide critical physical insights [24, 25]. Meanwhile, recent investigations have found that the wrinkled flamefront may exhibit non-locality, or "memory effects," in that the wrinkling is affected by local flow structure and the upstream flow conditions [3, 26]. Hemchandra and Lieuwen [27] demonstrated that such dynamics stem from the propagation of flamefront wrinkles in the direction of the mean tangential flow. The ambient pressure can significantly influence the wrinkling process. In particular, at higher pressures, the flamefront becomes thinner and, thus, exhibits finer corrugations [28-30]. On the other hand, the propagation and wrinkling of a turbulent flamefront also influence the upstream turbulence. Since the flamefront interacts with the turbulent eddies, a modification in flame geometry, and hence local heat release, can affect the local flow behavior. Such effects on turbulence have been characterized by changes in vorticity and strain rates [3, 31]. In a freely propagating flame, the flame may affect the flow field in its vicinity due to thermal expansion and the associated stretching of eddies, which can modify the turbulence characteristics of the flow [32]. This change is particularly pronounced in the normal direction, with isotropic turbulence in the upstream flow becoming altered to anisotropic turbulence in the post-flame region [33]. Furthermore, recent developments in 3D measurement techniques, including tomographic PIV [34–36], sparse particle flow velocimetry (SPFV) [37], high frequency swinging Mie-scattering [38, 39], have led to several new insights. These studies not only highlighted the structure of the flames in 3D space [36, 40], but also showed the three-dimensional effects on the important quantities

such as turbulent kinetic energy [34], flame speed [38, 41], and flame surface density [39].

The above short review of the literature demonstrates a few important findings. First, the global behavior of turbulent flames arises from the collective dynamics of local flamefronts, often termed flamelets. Furthermore, flame-turbulence interaction is a two-way coupled process. Hence, it is important to investigate the effect of the flame on the adjacent flow field, in addition to the commonly studied aspects of the influence of turbulence on the flame properties. The evaluation of flame-turbulence interaction becomes particularly critical for developing reduced-order models, where flame dynamics are captured in simple correlations and used as subgrid-scale models. Since the evolution of local statistics can be used as key parameters in quantifying flame-turbulence interaction, Lagrangian-based analyses gained interest among researchers. For example, Steinberg et al. [42] used Lagrangian tracking of fluid particles in turbulent flames to extract the evolution of principal strain rates. Hamlington et al. [43] used the Lagrangian particle tracking to show that fluid parcels follow a longer path in turbulent flames than laminar flames due to local flow straining. While these studies used fluid particles, there is another approach with fictitious particles, limiting the particle locations on flamefronts. Such an approach of tracking hypothetical flame particles is useful to study the local evolution of a flamefront. This approach was introduced by Pope [44] to analyze the evolution of properties of a hypothetical surface point on an isosurface in a turbulent flow, which moves relative to the fluid in the local normal direction to the surface. Subsequently, the propagation of the isosurface as it evolves was analyzed. As an extension of this concept, Chaudhuri [45] defined a *flame particle* as a surface point embedded and evolving on an isoscalar surface representing the flame. Despite the non-physical nature of such particles, the ability to track their movement enables the investigation of local changes in flame topology and its memory effects over time. This technique also facilitates the study of how incoming turbulence affects a flame element and allows for the identification of changes in properties on the flamefront, such as local stretch rate, which is critical for assessing the evolution of the flamefront. The study by Chaudhuri [45] on flame particle tracking in a turbulent premixed flame using direct numerical simulation revealed that these particles could experience a gradual increase in tangential strain rate and negative curvatures, ultimately leading to the local annihilation of the flame surface. Similarly, an experimental investigation utilizing the flame particle tracking on experiments of expanding premixed flames revealed distinct persistence time scales associated with the evolution of local curvature and strain rates [46].

In this study, we will explore key dynamics discussed in the above review within the context of a turbulent Bunsen flame. We aim to investigate the flame-turbulence interaction by studying local flow and flame statistics. This will be achieved by employing the high-speed velocity measurements performed on our turbulent flame in a Bunsen burner. First, we will assess how local turbulence is affected by flame propagation, comparing the statistics obtained with and without the flame. Next, we will quantify the flame-turbulence interaction by evaluating the statistics of three stretch rates conditioned on the flamefront. Finally, we will employ flame particle tracking to extract the progression of local stretch rates and delineate the characteristics and time scales associated with this evolution.

II. Experimental methodology and characterization

In this study, we use a piloted Bunsen burner with a nozzle diameter of 15.24mm to explore the dynamics of a premixed turbulent flame. The burner consists of a central tube that supplies the primary mixture and an annular slot for the co-flow. Turbulence in the unburned mixture was created by placing a stack of 3D-printed grids in the central tube upstream of the nozzle exit. The turbulence intensity could be varied by changing the number of grids in the stack. A premixed stoichiometric propane/oxygen/nitrogen (C₃H₈/O₂/N₂) mixture was supplied through the central tube and was ignited using a spark igniter to establish a stable flame. By changing the ratio of fuel and oxidizer (C₃H₈: O₂), the equivalence ratio of the mixture can be modulated. For this study, the stoichiometric (unity equivalence ratio) mixture was chosen to keep the Lewis number, defined as the ratio of thermal and mass diffusivity of the mixture, close to unity. The adiabatic flame temperature (T_b) was modulated by changing the oxygen-to-nitrogen ratio $(O_2 : N_2)$ in the mixture. Alicat mass-flow controllers were used to monitor and control the individual gas flow rates (Alicat MCR: ±0.2% full scale). Compared to laminar Bunsen flames, relatively high flow rates were required to establish a turbulent flame. In our experiments, the flow rate of 35SLPM was maintained, which resulted in a bulk velocity (\bar{U}) of 3.2m/s. At such flow rate, the flames are prone to blow off. To increase the stability and avoid blow-off, a pilot flame was created by burning a stoichiometric methane-air (21:79 of O₂ and N₂ moles) mixture at a low flow rate (10 SLPM) through the annular co-flow space. A constant flow rate of cooling water is supplied to the burner's inner channel to prevent overheating of its walls and protect it from damage. This cooling water also maintains the temperature of the premixed gas to remain constant throughout the experiments.

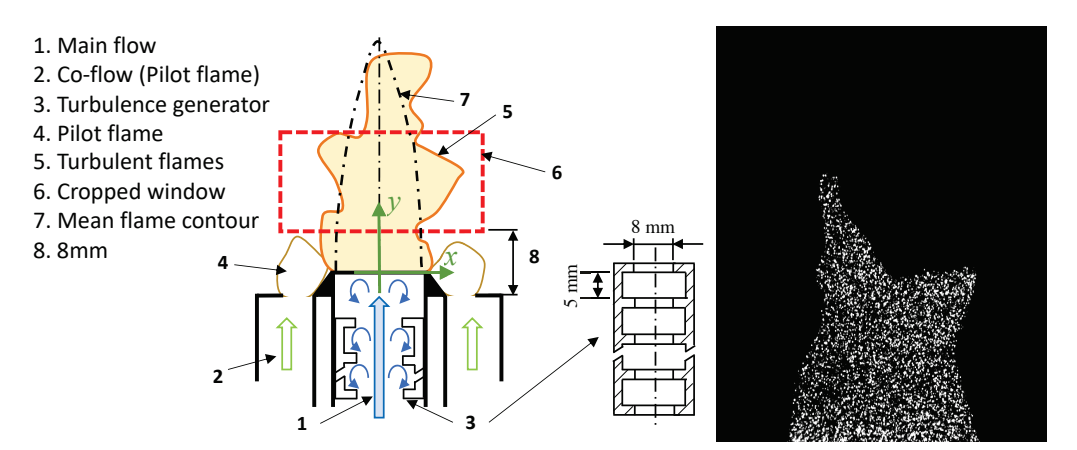


Fig. 1 Experimental setup: The schematic plot of the Bunsen burner and a sample Mie-scattering image of reactive flow.

We used Mie-scattering imaging and Particle Image Velocimetry (PIV) to visualize the dynamics of the turbulent flamefront and measure the flow velocities. The premixed gas in the main flow was seeded with Di-Ethyl-Hexyl-Sebacat (DEHS) droplets for this purpose. A high-speed dual-head Nd-YLF laser and necessary optics were used to create a vertical 2D laser sheet (Sheet thickness: FWHM: $\sim 400 \mu m$) placed above the burner as shown in Fig. 1. Our zone of

interest of the turbulent Bunsen flame had dimensions of 25×15 mm, which was located 8mm above the nozzle. This location was selected to minimize the influence of the pilot flame on the observed flame dynamics. A high-speed camera synchronized with laser pulses recorded the Mie-scattering images. The frame-straddled mode facilitated appropriate particle displacements between correlated image pairs, limiting errors in PIV measurements. Successive laser pulses were separated by a time interval of $50 \,\mu s$. Depending on the analysis, the frame rates for the data acquisition were changed between 500 to $18000 \, Hz$. To obtain the velocity vectors, the correlated Mie-scattering image pairs were processed using the PIV algorithm of LaVision's DaVis software with the final interrogation window size of 24 pixel $\times 24 \, \text{pixel} (\sim 720 \,\mu m \times 720 \,\mu m)$ with a 75% overlap. This results in approximately $180 \,\mu m$ spacing between PIV vectors. PIV was performed for both conditions, i.e., with flame (hot flow) and without flame (cold flow). Since the DEHS droplets evaporate near the flame, Mie-scattering images display a clear flame boundary (Fig. 1b), which was tracked using custom Matlab image processing codes. The identified flamefront is essentially the isothermal surface at which the droplets evaporate (close to the saturation temperature of DEHS). This method was previously used successfully to analyze the geometry and statistics of flamefronts [20, 46–49]. The concentration of the seeding droplet is small, and as such, their evaporation should not have significant effects on the flowfield.

This study investigated four flame/flow conditions using two levels of turbulent intensities (low, T_L , and high, T_H) and two different flame temperatures or oxygen percentages (low, O_L , and high, O_H). These conditions and their corresponding characteristics scales are detailed in Table. 1. According to previous studies, turbulent flames can be theoretically categorized into various regimes based on several important non-dimensional parameters [11, 50–52] including the turbulent Damköhler number, $Da = t_I/t_F$, the Karlovitz number, $Ka = t_F/t_\eta$, the turbulence intensity, u'_0/S_L , and the normalized length scales, L_I/δ_L , where t_I is the integral time scale, $t_F = \delta_L/S_L$ is the flame time scale, t_η is Kolmogorov time scale, u'_0 is RMS or turbulent velocity fluctuations, S_L is laminar flame speed and δ_L is the laminar flame thickness.

To obtain the fundamental flame properties, i.e., planar laminar flame speed (S_L) , flame thickness (δ_F) , a 1D Chemkin simulation of an unstretched laminar planer premixed flames was performed using *GRI-Mech 3.0* chemical mechanism [53]. Laminar flame thickness δ_F is calculated from the temperature profile of 1D unstretched laminar flames, $\delta_F = (T_b - T_u)/(dT/dx)_{max}$, where T_b is the burned flame temperature, T_u is the unburned flame temperature and $dT/dx|_{max}$ is the maximum temperature gradient [54]. The characteristics time scales for these flames, $t_F = \delta_F/S_L$, were also evaluated. The turbulence characteristics of the flow field can be quantified by the overall root mean square (r.m.s.) of velocity fluctuation, defined as

$$u'(x,y) = \sqrt{\frac{\left\langle \left(u_x(x,y) - \langle u_y(x,y)\rangle\right)^2\right\rangle + \left\langle \left(u_y(x,y) - \langle u_y(x,y)\rangle\right)^2\right\rangle}{2}}$$
(1)

Here, the instantaneous values of velocity components in transverse and axial directions are $u_x(x,y)$ and $u_y(x,y)$, respectively. $\langle u_x \rangle$ and $\langle u_y \rangle$ are their time-averaged values. We defined the origin of the coordinate system, i.e., x=0 and y=0 at the center of the nozzle exit. The global conditions from the nozzle were identified by the r.m.s. of velocity at the nozzle exit $u_0' = u'(0,0)$ (Eq. 1). The integral length scales $(\lambda_I)_{ij}$ were evaluated using the auto-correlation function of velocity fluctuations using the definitions from Pope [55]. The overall integral length scale, λ_I is defined as the mean of $(\lambda_I)_{ij}$, where i=x,y and j=x,y. The energy spectra from PIV measurements evaluated for the cold flow conditions showed a fully developed turbulence behavior, i.e., near -5/3 power-law dependence with the wavenumber [55]. Some of these spectra are shown in the supplementary material. The Kolmogorov timescale (t_η) is evaluated assuming self-similarity in dissipation of isotropic homogeneous turbulence, $\tau_\eta = (\nu \lambda_I/u_0')^3$ [55]. Here, ν is the kinematic viscosity of the premixed gas. We also evaluated the Karlovitz number $(Ka = t_F/t_\eta)$ to quantify the differences in timescales of flame and turbulence. The characteristic parameters for the four experimental conditions are listed in Table. 1.

Table 1 Relevant parameters of four experimental flame conditions, Re_T here is the turbulent Reynolds number, which is defined as $Re_T = u'_0 \lambda_I / v$

Condition	$\frac{O_2}{O_2+N_2}$	$ar{U}$	T_b	u_0'	S_L	t_F	δ_F	λ_I	t_{η}	Re_T	u_0'/S_L	Ka
		(m/s)	(K)	(m/s)	(m/s)	(ms)	(mm)	(mm)	(ms)			
T_LO_L	19%	3.2	2169	0.26	0.31	1.47	0.45	1.56	3.53	27	0.84	0.42
$T_L O_H$	21%	3.2	2271	0.26	0.40	0.94	0.37	1.56	3.64	27	0.65	0.26
$T_H O_L$	19%	3.2	2169	0.89	0.31	1.47	0.45	1.39	0.54	80	2.87	2.73
T_HO_H	21%	3.2	2271	0.89	0.40	0.94	0.37	1.39	0.56	80	2.22	1.67

III. Results and discussion

A. Flow statistics near the flamefront

To assess the effect of turbulence on flame dynamics, relevant quantities are often presented as functions of either turbulence intensity or r.m.s. of flow velocity. For example, one of the commonly used scaling relations for turbulent flame speed (S_T) is $S_T/S_L \approx (u_0'/S_L)^n$ [3, 9, 26], where u_0' is the r.m.s. of the turbulent flow field. For expanding turbulent flames, it was theoretically and experimentally shown that the normalized turbulent flame speed can be expressed as $S_T/S_L \approx \sqrt{(u_0'R_f)/(S_L\delta_L)}$ [30, 56, 57], where R_f is the mean radius for expanding flames. However, in these correlations, it is customary to use the u_0' measured for cold flow without the presence of flames. This is primarily due to the difficulty in performing the flow measurements in the presence of the flame in experiments. In theoretical analyses, the turbulence intensity is used as a fixed boundary condition and is commonly assumed to be constant. Moreover, for flame configurations that involve a burner and mean flow (e.g., jet flames or Bunsen flames), the measurements are performed at the nozzle exit, which may be far from the flame. Naturally, one question that arises

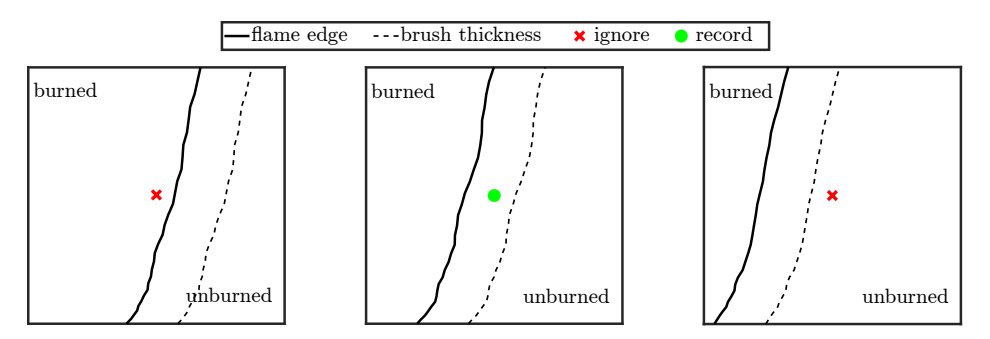


Fig. 2 An example of conditioned statistics: Data from a point was recorded only when it lies within the zone of influence.

from this discussion is whether the turbulence characteristics, especially r.m.s. of velocity, will remain the same if the measurements were to be performed for hot flow and in the vicinity of the flame locations. This will significantly impact the prediction of flame dynamics, as the correct evaluation of u' that the flame experiences is important. We will address and assess this possible mismatch by using the experimental data obtained in our experiments on turbulent Bunsen flames. Since our experimental method allows us to measure the velocity field in the upstream unburned mixture in the presence of the flame, we were able to quantify the effects of flame on the flow turbulence due to their interactions. We first extracted the flamefront locations from the Mie-scattering images using edge detection over a long time series to ensure statistical convergence. The mean flame location was then evaluated from the time-averaged flame position as a function of the vertical distance (y) from the burner exit. On the other hand, the standard deviation of the instantaneous flame locations at each y location was used to define the brush thickness (δ_T). We defined a zone of influence as an area that is located within the brush thickness $\pm \delta_T$) measured from the mean flame location. Next, we extracted the flow velocities (i.e., u_x and u_y) on the flamefront using PIV data and flame location identified from the Mie-scattering images. It is to be noted that due to the unsteadiness of the turbulent flame, the flamefront oscillates about the mean flame position. Since we are interested in the effects of flame on the flow, we limited our analysis only to the instances when the flamefront was located within the zone of influence, as shown in Fig. 2. Long duration for PIV measurements was used to ensure that the velocity time series contained more than 1000 data points for each spatial location, which ensured statistical convergence. Measurements were also carried out for cold-flow conditions, i.e., when the flame was absent.

Fig. 3 displays the spatial distributions (a) r.m.s. of velocity in the vicinity of the flame, u'_c and (b) r.m.s. of velocity at the same locations in the cold-flow, u' for low temperature and low turbulent condition (T_LO_L , see Table 1). Although there are small spatial variations in r.m.s. of velocity fluctuation, it is clear from the color maps that the r.m.s. of the velocity decreases in the presence of flame. This weakening can be associated with the thermal expansion effect. Thermal expansion creates a local flow in front of the flamefront, weakening upstream turbulence. To compare this reduction in turbulence strength across different experimental conditions, we plotted the ratio of r.m.s. of velocities with and without the flame (u'_c/u') measured along the mean flame location in Fig. 3c. We notice that the flame has

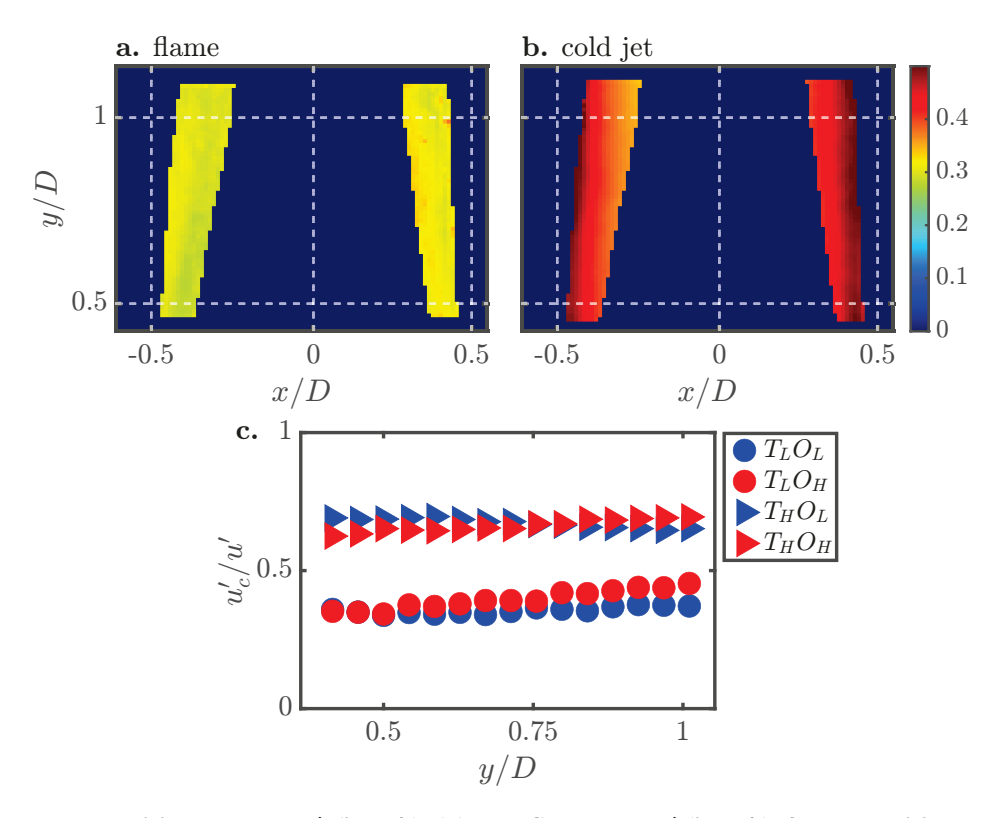


Fig. 3 (a) Flame-conditioned r.m.s. u'_c (in m/s), (b) cold flow r.m.s. u' (in m/s), from condition T_LO_L . (c) The ratio of u'_c/u' , along the mean flame location.

weakened the turbulence for all conditions, i.e., $u'_c/u' < 1$. Furthermore, for a given condition, the degree of weakening of turbulence seems to be constant along the flame and, hence, independent of distance from the nozzle (y/D). However, the degree of weakening does depend on the flame condition. Specifically, it is noticed that low turbulence conditions (both high and low flame temperature), i.e., T_LO_L and T_LO_H have significantly lower values of u'_c/u' , compared to high turbulence conditions, i.e., T_HO_L and T_HO_H . The relative strengths and responses of flame and turbulence can be quantified by the Karlovitz number (Ka), defined by the ratio of characteristic time scales. The T_LO_L and T_LO_H conditions have sub-unity Karlovitz number (Ka < 1), see Table 1), which denotes faster response time for flame compared to the turbulence. Thus, the damping effect of flame due to thermal expansion is stronger and hence lower u'_c/u' . On the other hand, for T_HO_L and T_HO_H conditions, the flame response is slower compared to the turbulence (Ka > 1), thus turbulence can resist the weakening effect induced by flame, leading to higher u'_c/u' . It is to be noted that the reduction in turbulence level can significantly decrease the effective Re_T . This may render a far field weakly turbulent flow condition laminar $(Re_T < 1)$ near the flamefront.

B. Local stretch rates

Next, we will analyze the statistics of flame stretch, which quantifies the rate of increase in flame surface area (A) and can be mathematically expressed as K = (1/A)dA/dt [58, 59]. As defined, the flame stretch rate can be broken

down into three components: the normal and tangential strain rates from the velocity gradient of the flow: K_n and K_t , and the stretch rate resulting from the curvature of the flame edge: K_c [60, 61].

$$K = \underbrace{S_{L\kappa}}_{K_c} + \underbrace{(-\mathbf{v} \cdot \mathbf{n})\kappa}_{K_n} + \underbrace{\nabla_t \cdot \mathbf{v}_t}_{K_t}$$
 (2)

where κ is the curvature of flamefront, v is local flow velocity, n it a unit vector normal to the flamefront, and subscript t denotes tangential direction. Since stretch rates quantify the changes in flamefront due to unsteady and non-uniform turbulent flow, their statistics can be used as a measure of flame-turbulence interactions [62]. In our study, as mentioned before, the edge of the flame in each Mie-scattering image is extracted by locating the maximum particle density gradient. The flamefront is then superimposed on the velocity vector field obtained from PIV. Once the flamefront geometry and the local instantaneous velocity vectors on the flamefront are obtained, the curvature and strain rates can be evaluated using Eq. 2. The probability distribution functions (PDFs) of each component of the stretch rate for all four experimental conditions are plotted in Fig. 4. In general, the stretch rates are affected by both turbulence and flame characteristics. Since we are interested in evaluating the effect of flame-turbulence interaction, we eliminated the pure effects of laminar flame dynamics (i.e., S_L and δ_F) by plotting a normalized stretch rate ($\tilde{K} = Kt_F$). The PDFs for all three stretch rates are symmetric, about 0. The PDFs also display long tails at extreme (high positive and negative) values. Such stretching of PDFs occurs due to intermittency, a hallmark of fully developed turbulence [63]. However, the width of the PDFs and the variance changes between different experimental conditions. This is further illustrated in Fig. 5, where we plotted the variance of K_c , K_n and K_t as function of Ka. It is apparent from the figure that the variance for all three stretch rates increases with Ka. For smaller $Ka = t_F/t_\eta$ conditions, the turbulence is relatively slower than flame propagation. This limits the degree of wrinkling of the flamefront and, hence, reduces the local non-uniformity in flame geometry and flow velocity. This also limits the stretch rates to a smaller range, resulting in a narrower PDF and smaller variance. With the increase in Ka, turbulence eddies become faster than flame propagation, imposing higher degrees of curvature and strains on the flamefront. This leads to wider PDFs and greater variance.

Next, we investigate the joint distribution of a pair of stretch rates to examine if there is any pairwise correlation between them. In Fig. 6, we show the scatter plots of two pairwise stretch rates, (a) \tilde{K}_n vs. \tilde{K}_t , and (b) \tilde{K}_c vs. \tilde{K}_n . The density of scatter points denotes the probability of the stretch rate values. These plots depict a clear pairwise link among the stretch rates. Figure 6a shows that the values of \tilde{K}_n and \tilde{K}_t follow almost a linear relation with a negative slope. To analyze these dynamics, we revisit the definitions of the stretch rates. The stretch rate due to the normal strain is defined as $K_n = (-\mathbf{v} \cdot \mathbf{n})\kappa$, where curvature, $\kappa = (-\nabla \cdot \mathbf{n})$. Thus, we can express, $K_n = (\mathbf{v} \cdot \mathbf{n})(\nabla \cdot \mathbf{n})$. On the other hand, the stretch rate due to tangential strain rate is defined as $K_t = \nabla_t \cdot \mathbf{v}_t = -\mathbf{n} \cdot \nabla \times (\mathbf{v} \times \mathbf{n})$, which can be rewritten as

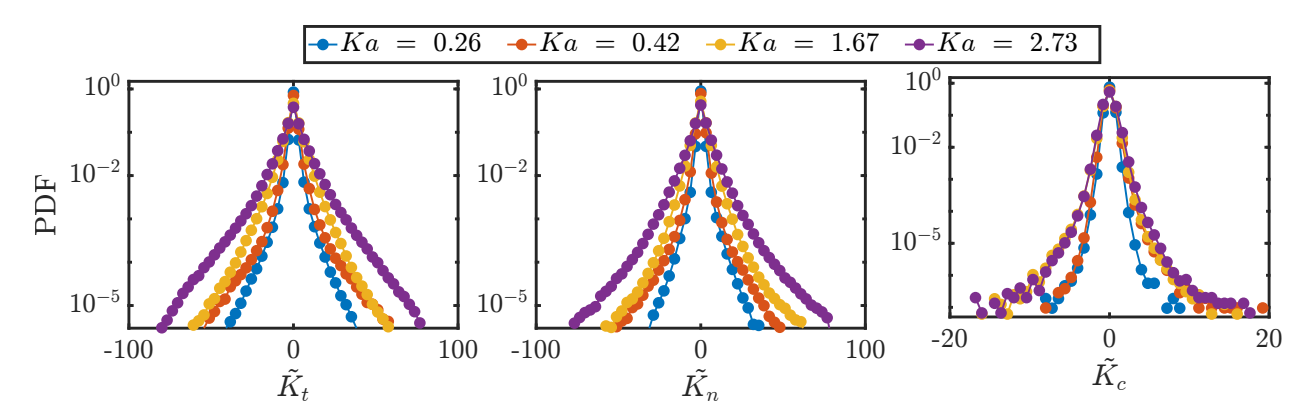


Fig. 4 The PDFs of normalized tangential strain rate (\tilde{K}_t) , normalized normal strain rate (\tilde{K}_n) , and normalized stretch due to curvature (\tilde{K}_c) .

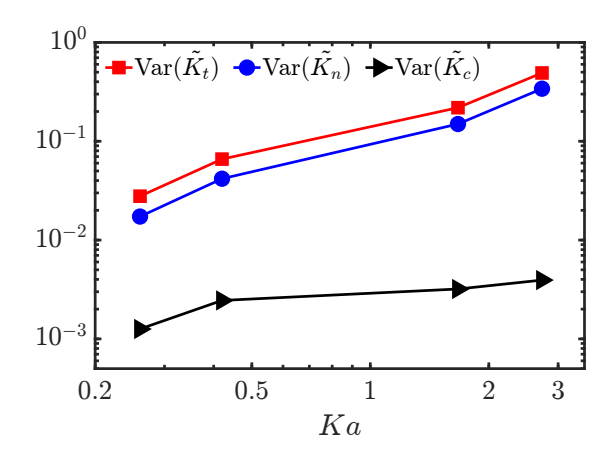


Fig. 5 The variances of (\tilde{K}_t) , (\tilde{K}_n) , and (\tilde{K}_c) for different Karlovitz numbers (Ka).

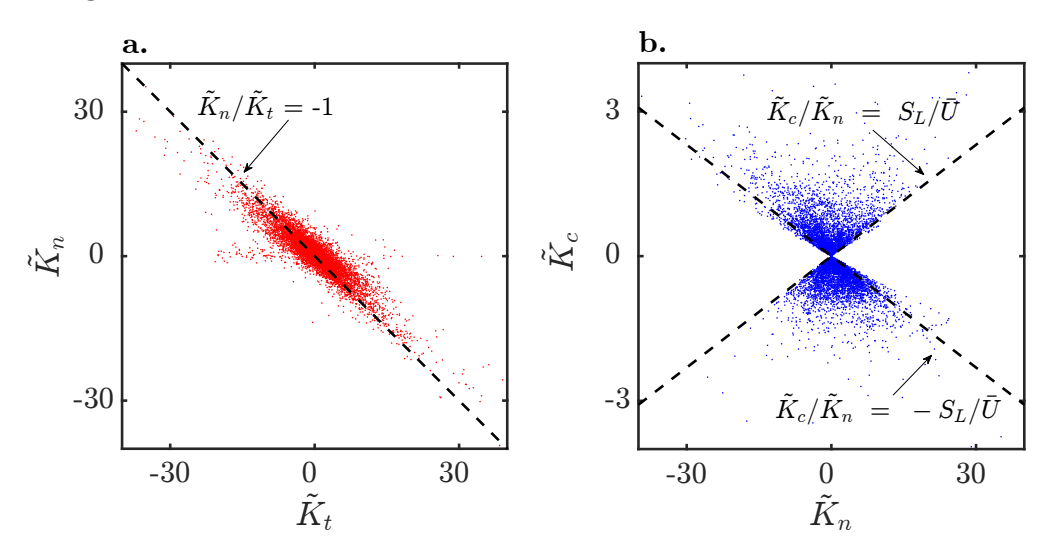


Fig. 6 Joint PDFs of different components of the stretch rate. The flame condition shown is $T_H O_L$

 $K_t = -(\mathbf{v} \cdot \mathbf{n})(\nabla \cdot \mathbf{n}) + (\nabla \cdot \mathbf{v})$. By comparing K_n and K_t , we find

$$K_t = -K_n + (\nabla \cdot \mathbf{v}) \tag{3}$$

Since the second term on the right-hand side, $\nabla \cdot \mathbf{v}$ is relatively small in a Bunsen flame, we expect K_n and K_t to be negatively correlated, i.e. $K_n \approx -K_t$. As shown in the figure, the slope between them is, indeed, close to -1. We also observe that the pairwise values of \tilde{K}_c and \tilde{K}_n are bounded by two lines (Figure 6b). Using their definitions, it can be shown that

$$\frac{K_n}{K_C} = -\frac{\mathbf{v} \cdot \mathbf{n}}{S_L}.\tag{4}$$

Here $\mathbf{v} \cdot \mathbf{n}$ is the normal component of the flow velocity on the flamefront. One can imagine that the maximum (and minimum) values of the mean flow velocity normal to the flamefront will be related to the flow velocity at the nozzle (\bar{U}) , or $-\bar{U} \leq \mathbf{v} \cdot \mathbf{n} \leq \bar{U}$. Based on these considerations, theoretical bounds for the pairwise scatter plot of K_c and K_n are defined by:

$$-\frac{S_L}{\bar{U}} \le \frac{K_c}{K_n} \le \frac{S_L}{\bar{U}} \tag{5}$$

where \bar{U} and S_L are constants for a given experiment.

C. Lagrangian statistics using flame particles

The PDFs of stretch rates, discussed and analyzed in the previous section, highlight the effect of turbulence on the local statistics. However, these statistics do not provide information on temporal evolution. For instance, while the PDFs reveal that an increase in turbulence level corresponds to broader values of stretch rates, they do not indicate how quickly the instantaneous stretch rate at a specific point on the flamefront changes. To answer this question, we need to analyze the temporal evolution of quantities at a location on the flamefront, generally obtained from Lagrangian statistics. In fluid dynamics, such analyses are often performed by tracking fluid particles, which move with the local flow velocity. However, in a turbulent flame, fluid particles do not remain on the flamefront, preventing the acquisition of statistics conditioned on the flamefront through particle tracking. Therefore, we will use the concept of flame particles. Flame particles are defined as a series of surface points that follow two rules: (1) they are always embedded on the flamefront, and (2) they co-move with it [44]. Since flame particles move with the flamefront, the time history of these particles and their properties (e.g., stretch rates, alignments) enable Lagrangian analysis. This, in turn, allows us to see how local segments of a flamefront evolve in time [45]. Flame particle tracking can be performed with great accuracy from the numerical simulation data due to its high temporal and spatial resolutions. While tracking from 2D high-speed PIV data is limited to the measurement plane, our previous study has shown that flame particle tracking from experimental data, which generally has lower spatial and temporal resolution than simulations, can still provide key insights [46].

In this study, to perform flame particle tracking using the 2D high-speed PIV data, we follow the methodology

outlined by Chaudhuri et al. [46]. The movement of a 2D surface particle can be described as [45]

$$\frac{d}{dt}\mathbf{X}_{2D}^{F}(t) = \mathbf{U}_{2D}\left(\mathbf{X}_{2D}^{F}[t], t\right) + S_d\left(\mathbf{X}_{2D}^{F}[t], t\right)\mathbf{n}_{2D}^{F}\left(\mathbf{X}_{2D}^{F}[t], t\right)$$
(6)

Here \mathbf{X}_{2D}^F is the location vector of a flame particle on the flamefront, \mathbf{U}_{2D} is the local velocity vector, \mathbf{n}_{2D}^F is the local surface normal, and S_d is the local displacement speed. The local displacement velocity can be calculated using the relation $S_d = S_L(1 + M_k \tilde{K})$, where M_k is the Markstein number. Further details of this tracking process can be found in [45]. Since the mixture used for this study has a Lewis number close to unity, we assume the Markstein number to be 0. We initiate a number of flame particles positioned on the flamefront near the bottom section of the flame and then allow them to evolve using Eq. 6. By identifying their locations on the flamefront and flame-conditioned variables (e.g., stretch rates) at each instance, we build a time series for each particle. This process was then repeated over a long series of the PIV data to obtain the temporal evolution of flame-conditioned statics.

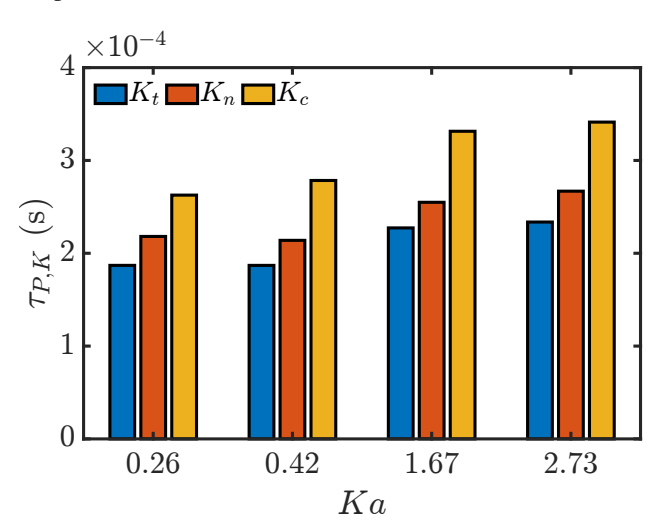


Fig. 7 Persistence time scale τ_{P,K_t} , τ_{P,K_n} , and τ_{P,K_c} for different conditions

To quantify the evolution or time history of the stretch rates conditioned on these flame particles, we computed the persistence timescale τ_P for each component of the stretch rate. The persistence time scale for stretch rates was calculated by integrating the auto-correlation function [46],

$$\tau_{P,K_i} = \overline{\int_0^\infty \left\langle \frac{K_i \left(\mathbf{X}_{2D}^F[t], t \right) \times K_i \left(\mathbf{X}_{2D}^F[t+\tau], t+\tau \right)}{\operatorname{var} \left(K_i \right)} \right\rangle d\tau}. \tag{7}$$

Here $K_i(t)$ is the i^{th} stretch rate $(i \in \{c, t, n\})$ measured for at an instance t on a flame particle. $\langle . \rangle$ and $\overline{(.)}$ denote averaging over time and various flame particles, respectively.

In the statistical sense, the persistence time scale denotes the duration for which a parameter's value remains sustained. In Fig. 7, we compare the τ_{P,K_t} , τ_{P,K_n} , and τ_{P,K_c} , for all four experimental conditions. A few interesting

observations can be made by comparing persistence time scales. First, we notice that, among the three components, τ_{P,K_c} consistently had the largest value, while τ_{P,K_t} had the smallest value, with a difference of a factor of about 1.5. This suggests that pure curvature is more persistent than tangential and normal strains. In other words, the local curvature of the flamefront resists changes due to local turbulent fluctuations, which is also reflected in smaller variances in the PDFs of $\tilde{K_c}$ (Fig. 5). On the other hand, the tangential strain rate is more responsive to turbulent fluctuations, and hence the shorter τ_{P,K_t} (Fig. 7) and larger variance in PDFs (Fig. 5). Moreover, we observe that the persistence time scales for all stretch rates increase with Ka. This suggests that, as the turbulence intensifies, the rate of decay for the local stretch rate slows down, which can be attributed to the weakened kinematic restoration [27]. Physically, the turbulence induces strains at multiple length scales, resulting in the wrinkling of the flamefront. As the flame propagates these wrinkles are gradually smoothed out. With an increase in Ka, the turbulence time scales become shorter than the flame time scales. Thus, the relaxation process due to flame propagation becomes slower, leading to longer persistent timescales.

D. Dispersion of flame particles and flamefront wrinkling

Next, we will analyze the dispersion of flame particles and relate them with local stretch in flamefronts. For Lagrangian fluid particle tracking in incompressible flows, it can be shown that the area (for 2D) or volume (for 3D) constructed by a fixed number of neighboring fluid particles remains constant. Thus, if the distance between two particles increases in one direction, it must decrease in at least one of the other two orthogonal directions. Based on this, the local stretching of fluid elements can be evaluated by tracking a set of fixed fluid particles in an unsteady, non-uniform flow. This approach has been used in many fluid problems to understand the underlying Lagrangian coherent structures (LCS) [64–66].

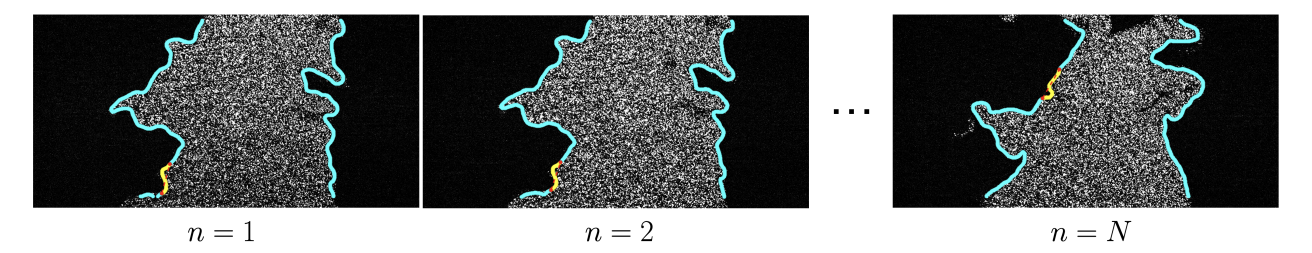


Fig. 8 A schematic of tracking neighboring particles.

Naturally, an immediate question arises: can the straining on the flamefront be evaluated similarly by tracking flame particles? We recognize that the flame particles have additional constraints compared to fluid particles, as the former is conditioned to be on the flamefront. Because of this, the area or volume conformed by the neighboring flame particles is not conserved or constant, and thus, an LCS type of analysis cannot be performed with flame particles. However, we can track the distance between the individual particle pairs and quantify their dispersion.

This can be achieved by positioning two flame particles on the flamefront at an initial time t = 0, then tracking

them until a fixed time, t = T. As the flame particles evolved, we recorded the length along the flamefront between the particle pairs, as shown in Fig. 8. We introduced the parameter "stretch factor", denoted as

$$\zeta = \frac{\Delta S_T}{\Delta S_0},\tag{8}$$

where ΔS_0 represents the initial length of the flamefront between the two flame particles, and ΔS_T corresponds to the length at time T. Physically, ζ represents the degree of extension or compression (straining) of the flame segment between a fixed flame particle pair. By tracking a large number of flame particle pairs spanning over a long time recording, we can build the statistics of ζ . Special consideration was taken in optimizing the selection of T. As time progresses, flame particles on a Bunsen flame typically migrate toward the flame's tip. For a very large T, the tracked flame particles may, eventually, leave the image plane. On the other hand, a short T will limit the evolution of local wrinkles or straining of the flamefront. Since the persistent time scales for all the stretches were found to be roughly around 0.2-0.35 ms, we used T=1ms. Note that we chose the value of T such that it is sufficiently long to induce flamefront wrinkling and facilitate statistical convergence yet short enough to prevent particle pairs from leaving the image plane. Moreover, we examined the selection of T=1ms and verified that slight changes in its value do not significantly influence the statistical results.

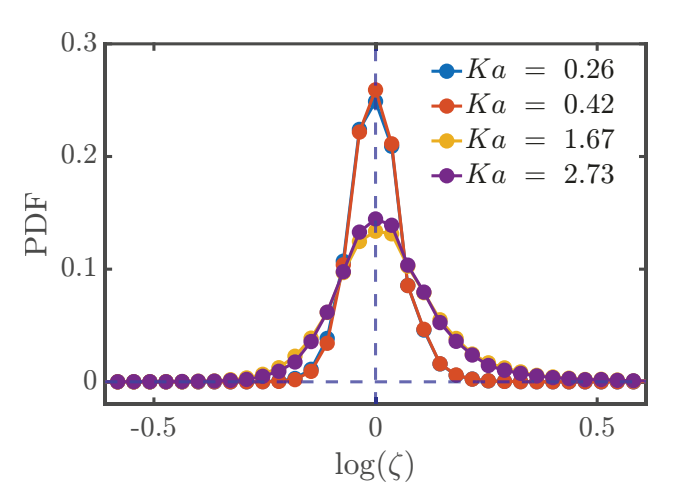


Fig. 9 PDF profile of stretch factor ξ , all four profiles follow a log-normal distribution.

In Fig. 9, we compare PDFs of the logarithm of ζ for all four experimental conditions. Several interesting observations can be made from the comparison. First, we note that ζ can have > 1 (log(ζ) > 0) and < 1 (log(ζ) < 0) values, i.e., the flame length between two paired flamed particles can increase and decrease. The wrinkling of the flamefront due to turbulent eddies can stretch the local flamefront positively and negatively, thereby increasing or decreasing the flamefront length (or surface area), respectively. The mechanism of generating and destroying the flame surface area and particles has been studied in detail for a statistically planar turbulent flame by Daveynate et al. [67].

Second, it is evident that ζ follows a log-normal distribution (or $\log(\zeta)$ follows a normal distribution) for all four conditions. In turbulence, the cascading processes of eddies drive dissipative processes (e.g., of kinetic energy), and they can be modeled as log-normal distributions [68, 69]. Later, it was shown that scalar quantities also follow a log-normal distribution [70]. Given that the generation and destruction of flamefronts in a turbulent flame are driven by eddies and their cascading processes, the PDFs of ζ display a log-normal distribution. Although kinematic restoration of flamefronts can be an additional mechanism for reducing wrinkled flamefronts, a log-normal distribution of ζ suggests a stronger effect of turbulent eddies. This is also evident from the third observation. The PDFs of ζ are almost identical across different T_b s for the same turbulence intensity or u'_0 . For example, the conditions of Ka=0.26 and 0.42 have lower u'_0 , and their PDFs of ζ are identical and narrower compared to the almost identical PDFs of Ka=1.637 and 2.73 conditions, which have higher u'_0 . As the u'_0 or the turbulent Reynolds number (Re_T) increases, the scales of energetic eddies increase, which leads to a broader distribution of wrinkling. Consequently, the profile of the log-normal distribution becomes wider. The lack of variations in the PDF of ζ at various T_b (and S_L) suggests that the turbulent eddies are the primary mechanism for extending and contracting flamefronts in our experimental conditions.

IV. Conclusion

In summary, we presented an experimental investigation of a turbulent Bunsen flame to evaluate various flameconditioned statistics to assess flame-turbulence interactions. Below, we summarize the major findings of our investigation.

- First, we compared the velocity statistics near the flamefront with the statistics of the cold flow. This revealed a decrease in local r.m.s of velocity due to the flame, which can be attributed to thermal expansion. Furthermore, we observed that stronger turbulence intensity or a larger Karlovitz number weakens this effect of flame.
- Next, we analyzed the PDFs of different stretch rates, which were evaluated from the experimental data. The PDFs show long tails, a feature often observed in statistics measured in turbulent flows due to intermittency. Moreover, due to the broadening of turbulent scales, the PDFs for stretch rates become wider with an increase in the Karlovitz number. Additionally, the joint scatter plots between pair-wise stretch rates display preferential distributions. The theoretical definitions of various stretch rates were then used to identify relations that describe such patterns.
- Finally, we used flame particle tracking to assess Lagrangian statistics. The temporal evolution of stretch rates conditioned on flame particles, which co-move with the flamefront, allows us to evaluate the persistent time scales. We found that the stretch rate due to curvature has a longer persistence time, making it the most resistant to change, compared to stretch rates due to normal and tangential strains. With an increase in Karlovitz number, the persistence time scale for all stretch rates increases due to the increased strength of turbulent eddies compared to flame propagation. By tracking the flame length between two flame particles over time, we also evaluated a stretch factor, which follows a log-normal distribution. This indicates that turbulence is the dominant mechanism

in controlling the wrinkling of the flames for the conditions explored in this study.

V. Acknowledgements

This work is supported by the US National Science Foundation (CBET-Grant number 2053671).

References

- [1] Pope, S. B., "Turbulent premixed flames," *Annual Review of Fluid Mechanics*, Vol. 19, No. 1, 1987, pp. 237–270. https://doi.org/10.1146/annurev.fl.19.010187.001321.
- [2] Fairweather, M., Ormsby, M., Sheppard, C., and Woolley, R., "Turbulent burning rates of methane and methane–hydrogen mixtures," *Combustion and Flame*, Vol. 156, No. 4, 2009, pp. 780–790. https://doi.org/10.1016/j.combustflame.2009.02.001.
- [3] Driscoll, J. F., "Turbulent premixed combustion: Flamelet structure and its effect on turbulent burning velocities," *Progress in Energy and Combustion Science*, Vol. 34, No. 1, 2008, pp. 91 134. https://doi.org/10.1016/j.pecs.2007.04.002.
- [4] Masri, A., Dibble, R., and Barlow, R., "The structure of turbulent nonpremixed flames revealed by Raman-Rayleigh-LIF measurements," *Progress in Energy and Combustion Science*, Vol. 22, No. 4, 1996, pp. 307–362. https://doi.org/10.1016/S0360-1285(96)00009-3.
- [5] Bell, J. B., Day, M. S., and Grcar, J. F., "Numerical simulation of premixed turbulent methane combustion," *Proceedings of the Combustion Institute*, Vol. 29, No. 2, 2002, pp. 1987–1993. https://doi.org/10.1016/S1540-7489(02)80242-5.
- [6] Bell, J. B., Day, M. S., Grear, J. F., Lijewski, M. J., Driscoll, J. F., and Filatyev, S. A., "Numerical simulation of a laboratory-scale turbulent slot flame," *Proceedings of the Combustion Institute*, Vol. 31, No. 1, 2007, pp. 1299–1307. https://doi.org/10.1016/j.proci.2006.07.186.
- [7] Filatyev, S. A., Driscoll, J. F., Carter, C. D., and Donbar, J. M., "Measured properties of turbulent premixed flames for model assessment, including burning velocities, stretch rates, and surface densities," *Combustion and Flame*, Vol. 141, No. 1-2, 2005, pp. 1–21. https://doi.org/10.1016/j.combustflame.2004.07.010.
- [8] Prasad, R., and Gore, J., "An evaluation of flame surface density models for turbulent premixed jet flames," *Combustion and Flame*, Vol. 116, No. 1-2, 1999, pp. 1–14. https://doi.org/10.1016/S0010-2180(98)00046-7.
- [9] Pitsch, H., "Large-eddy simulation of turbulent combustion," *Annual Review of Fluid Mechanics*, Vol. 38, 2006, pp. 453–482. https://doi.org/10.1146/annurev.fluid.38.050304.092133.
- [10] Clavin, P., "Dynamic behavior of premixed flame fronts in laminar and turbulent flows," *Progress in Energy and Combustion Science*, Vol. 11, No. 1, 1985, pp. 1–59. https://doi.org/10.1016/0360-1285(85)90012-7.
- [11] Peters, N., *Turbulent Combustion*, Cambridge Monographs on Mechanics, Cambridge University Press, 2000. https://doi.org/10.1017/CBO9780511612701.

- [12] Borghi, R., "Turbulent combustion modelling," *Progress in Energy and Combustion Science*, Vol. 14, No. 4, 1988, pp. 245–292. https://doi.org/10.1016/0360-1285(88)90015-9.
- [13] Poludnenko, A. Y., and Oran, E. S., "The interaction of high-speed turbulence with flames: Global properties and internal flame structure," *Combustion and Flame*, Vol. 157, No. 5, 2010, pp. 995–1011. https://doi.org/10.1016/j.combustflame.2009.11.018.
- [14] Skiba, A. W., Wabel, T. M., Carter, C. D., Hammack, S. D., Temme, J. E., and Driscoll, J. F., "Premixed flames subjected to extreme levels of turbulence part I: Flame structure and a new measured regime diagram," *Combustion and Flame*, Vol. 189, 2018, pp. 407–432. https://doi.org/10.1016/j.combustflame.2017.08.016.
- [15] Liu, Z., Unni, V. R., Chaudhuri, S., Law, C. K., and Saha, A., "Local statistics of laminar expanding flames subjected to Darrieus–Landau instability," *Proceedings of the Combustion Institute*, Vol. 38, No. 2, 2021, pp. 1993–2000. https://doi.org/10.1016/j.proci.2020.06.118.
- [16] Weng, Y., Potnis, A., and Saha, A., "Regime and morphology of polyhedral Bunsen flames," *Combustion and Flame*, Vol. 248, 2023, p. 112585. https://doi.org/10.1016/j.combustflame.2022.112585.
- [17] Steinberg, A., Driscoll, J., and Ceccio, S., "Temporal evolution of flame stretch due to turbulence and the hydrodynamic instability," *Proceedings of the Combustion Institute*, Vol. 32, No. 2, 2009, pp. 1713–1721. https://doi.org/10.1016/j.proci.2008.05.003.
- [18] Chaudhuri, S., Akkerman, V., and Law, C. K., "Spectral formulation of turbulent flame speed with consideration of hydrodynamic instability," *Physical Review E*, Vol. 84, No. 2, 2011, p. 026322. https://doi.org/10.1103/PhysRevE.84.026322.
- [19] Yang, S., Saha, A., Liu, Z., and Law, C. K., "Role of Darrieus–Landau instability in propagation of expanding turbulent flames," *Journal of Fluid Mechanics*, Vol. 850, 2018, pp. 784–802. https://doi.org/10.1017/jfm.2018.426.
- [20] Liu, Z., Yang, S., Law, C. K., and Saha, A., "Cellular instability in *Le* < 1 turbulent expanding flames," *Proceedings of the Combustion Institute*, Vol. 37, No. 2, 2019, pp. 2611–2618. https://doi.org/10.1016/j.proci.2018.07.056.
- [21] Charlette, F., Meneveau, C., and Veynante, D., "A power-law flame wrinkling model for LES of premixed turbulent combustion Part I: non-dynamic formulation and initial tests," *Combustion and Flame*, Vol. 131, No. 1-2, 2002, pp. 159–180. https://doi.org/10.1016/S0010-2180(02)00400-5.
- [22] Weller, H., Tabor, G., Gosman, A., and Fureby, C., "Application of a flame-wrinkling LES combustion model to a turbulent mixing layer," *Symposium (international) on Combustion*, Vol. 27, Elsevier, 1998, pp. 899–907. https://doi.org/10.1016/S0082-0784(98)80487-6.
- [23] Hawkes, E. R., Chatakonda, O., Kolla, H., Kerstein, A. R., and Chen, J. H., "A petascale direct numerical simulation study of the modelling of flame wrinkling for large-eddy simulations in intense turbulence," *Combustion and Flame*, Vol. 159, No. 8, 2012, pp. 2690–2703. https://doi.org/10.1016/j.combustflame.2011.11.020.

- [24] Mueller, C. J., Driscoll, J. F., Reuss, D. L., Drake, M. C., and Rosalik, M. E., "Vorticity generation and attenuation as vortices convect through a premixed flame," *Combustion and Flame*, Vol. 112, No. 3, 1998, pp. 342–358. https://doi.org/10.1016/S0010-2180(97)00122-3.
- [25] Renard, P.-H., Thevenin, D., Rolon, J.-C., and Candel, S., "Dynamics of flame/vortex interactions," *Progress in Energy and Combustion Science*, Vol. 26, No. 3, 2000, pp. 225–282. https://doi.org/10.1016/S0360-1285(00)00002-2.
- [26] Lipatnikov, A., and Chomiak, J., "Turbulent flame speed and thickness: phenomenology, evaluation, and application in multi-dimensional simulations," *Progress in Energy and Combustion Science*, Vol. 28, No. 1, 2002, pp. 1–74. https://doi.org/10.1016/S0360-1285(01)00007-7.
- [27] Hemchandra, S., and Lieuwen, T., "Local consumption speed of turbulent premixed flames—An analysis of "memory effects"," *Combustion and Flame*, Vol. 157, No. 5, 2010, pp. 955–965. https://doi.org/10.1016/j.combustflame.2009.10.007.
- [28] Kobayashi, H., Nakashima, T., Tamura, T., Maruta, K., and Niioka, T., "Turbulence measurements and observations of turbulent premixed flames at elevated pressures up to 3.0 MPa," *Combustion and Flame*, Vol. 108, No. 1-2, 1997, pp. 104–117. https://doi.org/10.1016/S0010-2180(96)00103-4.
- [29] Kobayashi, H., Seyama, K., Hagiwara, H., and Ogami, Y., "Burning velocity correlation of methane/air turbulent premixed flames at high pressure and high temperature," *Proceedings of the Combustion Institute*, Vol. 30, No. 1, 2005, pp. 827–834. https://doi.org/10.1016/j.proci.2004.08.098.
- [30] Wu, F., Saha, A., Chaudhuri, S., and Law, C. K., "Propagation speeds of expanding turbulent flames of C4 to C8 n-alkanes at elevated pressures: Experimental determination, fuel similarity, and stretch-affected local extinction," *Proceedings of the Combustion Institute*, Vol. 35, No. 2, 2015, pp. 1501–1508. https://doi.org/10.1016/j.proci.2014.07.070.
- [31] Liu, Z., Unni, V. R., Chaudhuri, S., Sui, R., Law, C. K., and Saha, A., "Self-turbulization in cellularly unstable laminar flames," *Journal of Fluid Mechanics*, Vol. 917, 2021, p. A53. https://doi.org/10.1017/jfm.2021.330.
- [32] Pope, S. B., "PDF methods for turbulent reactive flows," *Progress in Energy and Combustion Science*, Vol. 11, No. 2, 1985, pp. 119–192. https://doi.org/10.1016/0360-1285(85)90002-4.
- [33] Videto, B., and Santavicca, D., "Flame-turbulence interactions in a freely-propagating, premixed flame," *Combustion Science and Technology*, Vol. 70, No. 1-3, 1990, pp. 47–73. https://doi.org/10.1080/00102209008951611.
- [34] Baum, E., Peterson, B., Surmann, C., Michaelis, D., Böhm, B., and Dreizler, A., "Investigation of the 3D flow field in an IC engine using tomographic PIV," *Proceedings of the Combustion Institute*, Vol. 34, No. 2, 2013, pp. 2903–2910. https://doi.org/10.1016/j.proci.2012.06.123.
- [35] Liu, N., Zhou, K., and Ma, L., "3D tomography integrating view registration and its application in highly turbulent flames," *Combustion and Flame*, Vol. 221, 2020, pp. 429–440. https://doi.org/10.1016/j.combustflame.2020.08.025.

- [36] Ebi, D., and Clemens, N. T., "Simultaneous high-speed 3D flame front detection and tomographic PIV," Measurement Science and Technology, Vol. 27, No. 3, 2016, p. 035303. https://doi.org/10.1088/0957-0233/27/3/035303.
- [37] Lu, G., Steinberg, A., and Yano, M., "A sparse optical flow inspired method for 3D velocimetry," *Experiments in Fluids*, Vol. 64, No. 4, 2023, p. 66. https://doi.org/10.1007/s00348-023-03593-z.
- [38] Ahmed, P., Thorne, B., Lawes, M., Hochgreb, S., Nivarti, G. V., and Cant, R. S., "Three dimensional measurements of surface areas and burning velocities of turbulent spherical flames," *Combustion and Flame*, Vol. 233, 2021, p. 111586. https://doi.org/10.1016/j.combustflame.2021.111586.
- [39] Zheng, Y., Weller, L., and Hochgreb, S., "3D flame surface measurements in low-turbulence Bunsen flames via scanning and orthogonal cross-planar techniques," *Combustion and Flame*, Vol. 258, 2023, p. 113103. https://doi.org/10.1016/j.combustflame. 2023.113103.
- [40] Trueba-Monje, I., and Sutton, J. A., "Flame structure and broadening in turbulent premixed jet flames," *Combustion and Flame*, Vol. 251, 2023, p. 112676. https://doi.org/10.1016/j.combustflame.2023.112676.
- [41] Chakraborty, N., Hartung, G., Katragadda, M., and Kaminski, C., "Comparison of 2D and 3D density-weighted displacement speed statistics and implications for laser based measurements of flame displacement speed using direct numerical simulation data," *Combustion and Flame*, Vol. 158, No. 7, 2011, pp. 1372–1390. https://doi.org/https://doi.org/10.1016/j.combustflame. 2010.11.014.
- [42] Steinberg, A. M., Coriton, B., and Frank, J., "Influence of combustion on principal strain-rate transport in turbulent premixed flames," *Proceedings of the Combustion Institute*, Vol. 35, No. 2, 2015, pp. 1287–1294. https://doi.org/10.1016/j.proci.2014.06. 089.
- [43] Hamlington, P. E., Darragh, R., Briner, C. A., Towery, C. A., Taylor, B. D., and Poludnenko, A. Y., "Lagrangian analysis of high-speed turbulent premixed reacting flows: Thermochemical trajectories in hydrogen–air flames," *Combustion and Flame*, Vol. 186, 2017, pp. 193–207. https://doi.org/10.1016/j.combustflame.2017.08.001.
- [44] Pope, S., "The evolution of surfaces in turbulence," *International Journal of Engineering Science*, Vol. 26, No. 5, 1988, pp. 445 469. https://doi.org/10.1016/0020-7225(88)90004-3.
- [45] Chaudhuri, S., "Life of flame particles embedded in premixed flames interacting with near isotropic turbulence," *Proceedings of the Combustion Institute*, Vol. 35, No. 2, 2015, pp. 1305 1312. https://doi.org/10.1016/j.proci.2014.08.007.
- [46] Chaudhuri, S., Saha, A., and Law, C. K., "On flame–turbulence interaction in constant-pressure expanding flames," *Proceedings of the Combustion Institute*, Vol. 35, No. 2, 2015, pp. 1331 1339. https://doi.org/10.1016/j.proci.2014.07.038.
- [47] Upatnieks, A., Driscoll, J. F., Rasmussen, C. C., and Ceccio, S. L., "Liftoff of turbulent jet flames—assessment of edge flame and other concepts using cinema-PIV," *Combustion and Flame*, Vol. 138, No. 3, 2004, pp. 259–272. https://doi.org/10.1016/j.combustflame.2004.04.011.

- [48] Weinkauff, J., Michaelis, D., Dreizler, A., and Böhm, B., "Tomographic PIV measurements in a turbulent lifted jet flame," *Experiments in Fluids*, Vol. 54, 2013, pp. 1–5. https://doi.org/10.1007/s00348-013-1624-1.
- [49] Saha, A., Chaudhuri, S., and Law, C. K., "Flame surface statistics of constant-pressure turbulent expanding premixed flames," *Physics of Fluids*, Vol. 26, No. 4, 2014. https://doi.org/10.1063/1.4871021.
- [50] Borghi, R., "On the structure and morphology of turbulent premixed flames," *Recent Advances in the Aerospace Sciences*, Springer, 1985, pp. 117–138. https://doi.org/10.1007/978-1-4684-4298-4_7.
- [51] Abdel-Gayed, R., Bradley, D., and Lung, F.-K., "Combustion regimes and the straining of turbulent premixed flames," *Combustion and Flame*, Vol. 76, No. 2, 1989, pp. 213–218. https://doi.org/10.1016/0010-2180(89)90068-0.
- [52] Poinsot, T., veyynante, D., and Candel, S., "Diagrams of premixed turbulent combustion based on direct simulation," *Symposium* (*international*) on *Combustion*, Vol. 23, Elsevier, 1991, pp. 613–619. https://doi.org/10.1016/S0082-0784(06)80308-5.
- [53] Smith, G. P., Golden, D. M., Frenklach, M., Moriarty, N. W., Eiteneer, B., Goldenberg, M., Bowman, C. T., Hanson, R. K., Song, S., Gardiner, W. C., and et al., "GRI 3.0,", 1999. URL http://www.me.berkeley.edu/gri_mech/.
- [54] Poinsot, T., and Veynante, D., *Theoretical and numerical combustion*, RT Edwards, Inc., 2005. URL https://books.google.com/books/about/Theoretical_and_Numerical_Combustion.html?id=cqFDkeVABYoC.
- [55] Pope, S. B., Turbulent flows, Cambridge university press, 2000. https://doi.org/10.1017/CBO9780511840531.
- [56] Chaudhuri, S., Wu, F., Zhu, D., and Law, C. K., "Flame speed and self-similar propagation of expanding turbulent premixed flames," *Physical Review Letters*, Vol. 108, No. 4, 2012, p. 044503. https://doi.org/10.1103/PhysRevLett.108.044503.
- [57] Nguyen, M., Yu, D., and Shy, S., "General correlations of high pressure turbulent burning velocities with the consideration of Lewis number effect," *Proceedings of the Combustion Institute*, Vol. 37, No. 2, 2019, pp. 2391–2398. https://doi.org/10.1016/j. proci.2018.08.049.
- [58] Williams, F., "Recent advances in theoretical descriptions of turbulent diffusion flames," *Turbulent Mixing in Nonreactive and Reactive Flows*, 1975, pp. 189–208. https://doi.org/10.1007/978-1-4615-8738-5_5.
- [59] Law, C. K., Combustion Physics, Cambridge University Press, 2006. https://doi.org/10.1017/CBO9780511754517.
- [60] Matalon, M., "On flame stretch," Combustion Science and Technology, Vol. 31, No. 3-4, 1983, pp. 169–181. https://doi.org/10.1080/00102208308923638.
- [61] Candel, S. M., and Poinsot, T. J., "Flame stretch and the balance equation for the flame area," *Combustion Science and Technology*, Vol. 70, No. 1-3, 1990, pp. 1–15. https://doi.org/10.1080/00102209008951608.
- [62] Creta, F., and Matalon, M., "Propagation of wrinkled turbulent flames in the context of hydrodynamic theory," *Journal of Fluid Mechanics*, Vol. 680, 2011, pp. 225–264. https://doi.org/10.1017/jfm.2011.157.

- [63] Lohse, D., and Grossmann, S., "Intermittency in turbulence," *Physica A: Statistical Mechanics and its Applications*, Vol. 194, No. 1-4, 1993, pp. 519–531. https://doi.org/10.1016/0378-4371(93)90382-E.
- [64] Haller, G., and Yuan, G., "Lagrangian coherent structures and mixing in two-dimensional turbulence," *Physica D: Nonlinear Phenomena*, Vol. 147, No. 3-4, 2000, pp. 352–370. https://doi.org/10.1016/S0167-2789(00)00142-1.
- [65] Haller, G., "Distinguished material surfaces and coherent structures in three-dimensional fluid flows," *Physica D: Nonlinear Phenomena*, Vol. 149, No. 4, 2001, pp. 248–277. https://doi.org/10.1016/S0167-2789(00)00199-8.
- [66] Haller, G., "Lagrangian coherent structures," *Annual Review of Fluid Mechanics*, Vol. 47, 2015, pp. 137–162. https://doi.org/10.1146/annurev-fluid-010313-141322.
- [67] Daveynate, H. L., Mohan, A., and Chaudhuri, S., "Genesis and evolution of premixed flames in turbulence," *Combustion and Flame*, Vol. 196, 2018, pp. 386–399. https://doi.org/10.1016/j.combustflame.2018.06.030.
- [68] Kolmogorov, A. N., "A refinement of previous hypotheses concerning the local structure of turbulence in a viscous incompressible fluid at high Reynolds number," *Journal of Fluid Mechanics*, Vol. 13, No. 1, 1962, pp. 82–85. https://doi.org/10.1017/S0022112062000518.
- [69] Obukhov, A., "Some specific features of atmospheric turbulence," *Journal of Geophysical Research*, Vol. 67, No. 8, 1962, pp. 3011–3014. https://doi.org/10.1029/JZ067i008p03011.
- [70] Antonia, R. A., and Sreenivasan, K. R., "Log-normality of temperature dissipation in a turbulent boundary layer," *Physics of Fluids*, Vol. 20, No. 11, 1977, pp. 1800–1804. https://doi.org/10.1063/1.861795.